Journal of Applied Polymer Science

The Study of Char Forming on OPS/PC and DOPO-POSS/PC Composites

Baofa Cheng, Wenchao Zhang, Xiangmei Li, Rongjie Yang
School of Material Science and Engineering, National Laboratory of Flame Retardant Materials, Engineering Research Center of Fire-Safe Materials and Technology, Ministry of Education, Beijing Institute of Technology, Beijing 100081, People's Republic of China
Correspondence to: X. Li (E-mail: bjlglxm@bit.edu.cn)

ABSTRACT: Polyhedral oligomeric octaphenyl silsesquioxane (OPS) and polyhedral oligomeric silsesquioxane containing 9,10-dihydro-9-oxa-10-phosphaphenanthrene-10-oxide (DOPO-POSS) with polycarbonate (PC) were each prepared by twin screw extrusion. Their flammability was studied by cone calorimetry under different heat fluxes (35 and 50 kW/m^2). In the cone calorimeter testing, thermocouples were used to measure the temperature at the top and bottom of the composites. Compared to the DOPO-POSS/PC composite, the char layer of the OPS/PC composite is better for preventing heat transfer, the temperature change indicates that OPS/PC composite has a longer period of char formation, and the organization of their char materials are different. The DOPO-POSS/PC composite has a harder char layer than the OPS/PC composite, but the OPS/PC composite char layer is more compact. The char layer macrostructure was studied with scanning electron microscopy (SEM) and EDS, which indicated that there are many bubbles and pores in the DOPO-POSS/PC composite. EDS showed that there was some Si content in the exterior and interior char for the DOPO-POSS/PC composite; there is a greater Si content in the exterior OPS/PC char residue than in the interior. The storage modulus of OPS/PC composite was higher than the PC control and DOPO-POSS/PC composite at low frequencies. The values of η^* of the OPS/PC composite were higher than the PC control and DOPO-POSS/PC composite at low frequencies; also, the PC control exhibits a quasi-Newtonian regime, but the OPS/PC and DOPO-POSS/PC composites exhibit typical shear-thinning behavior. © 2013 Wiley Periodicals, Inc. J. Appl. Polym. Sci. **2014**, *131*, 39892.

KEYWORDS: PC; OPS; DOPO-POSS; flammability; rheology

Received 26 March 2013; accepted 27 August 2013
DOI: 10.1002/app.39892

INTRODUCTION

Bisphenol A polycarbonate (PC) is one of the most important commercial aromatic polycarbonates because of its excellent properties, such as its transparency, high mechanical strength, good thermal stability, and flame retardancy.[1,2] PC is an amorphous polymer with a relatively high glass transition temperature (T_g = 140–150°C). PC exhibits a V-2 rating in the UL-94 test because PC is a naturally high charring polymer. However, more rigorous flame retardant performance is often required for electronic and electrical applications.[1,3]

Polyhedral oligomeric silsesquioxanes (POSS) have a cage-like structure that is 1–3 nm in size. Their chemical composition can be represented as $(RSiO_{1.5})_n$ which lies between silica and silicones $(R_2SiO)_x$, where R can be hydrogen, any alkyl, alkylene, aryl, or arylene group, or organo-functional derivatives.[4–7] POSS is an organic–inorganic hybrid material. It combines the thermal stability of inorganic materials with the advantages of organic materials. Many scientific articles have been published on the use of POSS as flame retardants. Incorporation of POSS can lead to dramatic improvement of some properties of composites, such as increases in use temperature, oxidation resistance, as well as reductions in flammability and viscosity of materials during processing.[8–10] The V-0 rating in the UL-94 test can be obtained with the addition of OPS at 6 and 4 wt % in our previous works.[11–13]

The authors analyzed the char formation of OPS/PC and DOPO-POSS composites, and some novel points are discussed in this article. The temperature change between top and bottom layer of the material, the process and the mechanism of char formation during the cone test and the char strength were investigated; such information is rarely mentioned by other researchers. 4 wt % DOPO-POSS/PC and 6 wt % OPS/PC composites were prepared. Both composites could reach the V-0 burning rate, and the composites each developed char layer structures at 35 and 50 kW/m^2 according to cone calorimetry.

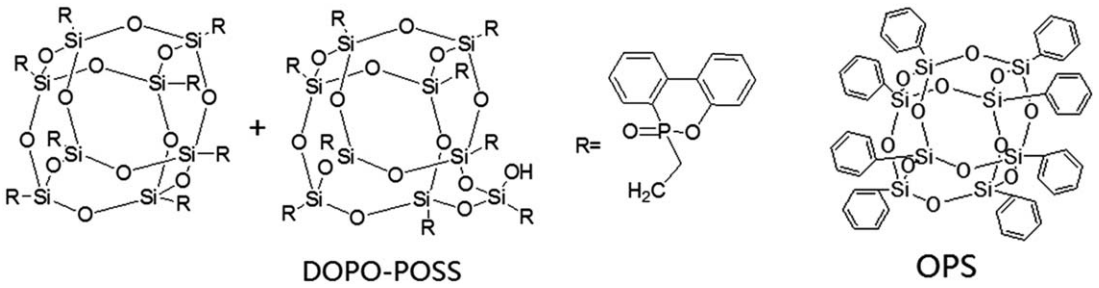

Scheme 1. Molecular structures of DOPO-POSS and OPS.

Heat release rate (HRR) and total heat release (THR), the temperature changes between the top and bottom surfaces, the exterior and interior char morphology, the char residue component, char strength, and the rheological behavior of the two different composites were studied.

EXPERIMENTAL

Materials

OPS and DOPO-POSS were synthesized in our lab.[12] PC was Makrolon 2805, purchased from Bayer Material Science. Their molecular structures are shown in Scheme 1.

Composite Preparation

Prior to compounding, the PC pellets were dried for at least 5 h under a hot air circulating oven at 120°C; the OPS and DOPO-POSS were dried for at least 2 h under a hot air circulating oven at 120 and 80°C respectively. The composites were prepared by blending PC with either 6 wt % OPS or 4 wt % DOPO-POSS, and then adding 0.3 wt % PTFE, a small amount of antioxidant 1010 and antioxidant 168 in a SJ-20 twin-screw extruder (screw diameter $\Phi = 20$ mm; length to diameter, $L/D = 40$). The OPS/PC and DOPO-POSS pellets were dried and used to prepare different test samples by means of an injection molding machine (HTF90X1, Haitian Plastics Machinery).

Measurements

Combustion experiments were performed on a cone calorimeter device (Fire Testing Technology) according to the ISO-5660-1:2002 standard. The dimensions of the samples were 100 mm × 100 mm × 3 mm and the heat fluxes were 35 and 50 kW/m^2. The samples were wrapped in tin foil while leaving the upper surface exposed to the radiator, and the ceramic backing board was set 25 mm from the cone base. The results reported were the averages of three repeated experiments.

Two thermocouples were plugged into the top and bottom of the sample, respectively, to record the temperature changes.

Rheological behavior studies were carried out on a controlled strain rheometer (RS300; Thermo HAAKE Scientific). Measurements were performed in the plate–plate configuration with a gap of 1.0 mm. The sensor type was a PP20 Ti. Oscillation frequency sweep tests were performed on the PC as well as on 6 wt % OPS/PC and 4 wt % DOPO-POSS/PC composites at 290°C. The range of ω was 0.01∼100 rad/s, and $\tau = 1$ Pa.

The char layer strength was measured by a controlled strain rheometer (RS300, Thermo HAAKE Scientific). The char layer was placed in the plate–plate configuration with a gap of 23 mm. The dimensions of the char layer were about 20 mm × 20 mm × 22 mm. The plate moved from 23 mm to 5 mm and the measurement test time was 60 s.

Scanning electron microscopy (SEM) experiments were performed with a Hitachi S-4800 scanning electron microscope. Char residues for SEM were prepared by cone and surface sputtering with gold.

RESULTS AND DISCUSSION

Heat Flux versus Thermocouple Temperature

Temperature measurements were carried out at the different heat fluxes (35 and 50 kW/m^2) during the cone test. Figures 1 and 2 present the measured temperature curves at the top and bottom surfaces of the PC control, DOPO-POSS/PC, and OPS/PC composites with incident heat fluxes of 35 and 50 kW/m^2. The temperature was collected every 10 s from when the composites melted until complete flameout.

Cone results for the PC control, DOPO-POSS/PC, and OPS/PC composites are listed in Table I.

In Table I, at 50kW/m^2, the TTI of the PC control, DOPO-POSS/PC, and OPS/PC composites are 97 s, 95 s, and 80 s, respectively, and all of them are shorter than at 35 kW/m^2. The OPS/PC time to flameout (TTF) is longer than both the PC control and DOPO-POSS/PC composite. At 35 and 50 kW/m^2,

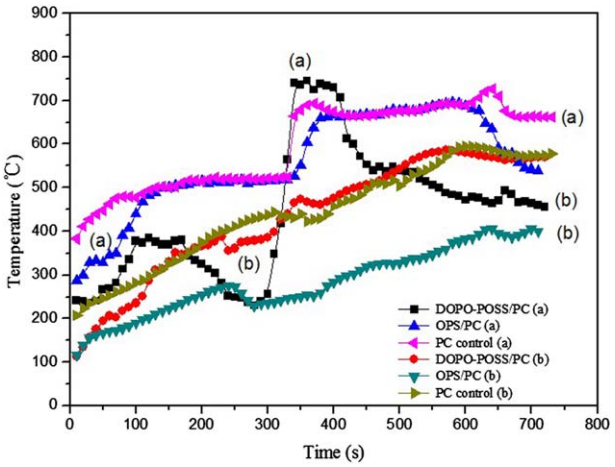

Figure 1. Measured temperature curves about the top (a) and bottom (b) of PC control, DOPO-POSS/PC and OPS/PC composites (35 kW/m^2). [Color figure can be viewed in the online issue, which is available at wileyonlinelibrary.com.]

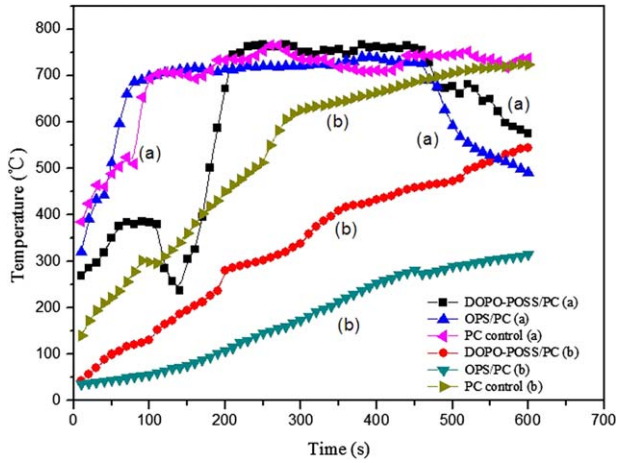

Figure 2. Measured temperature curves about the top (a) and bottom (b) of PC control, DOPO-POSS/PC and OPS/PC composites (50 kW/m^2). [Color figure can be viewed in the online issue, which is available at wileyonlinelibrary.com.]

the peak heat rate release of the OPS/PC and DOPO-POSS/PC composites are lower than that of the PC control. The peak of heat release rate (PHRR) of the OPS/PC composite is less 40% than that of the DOPO-POSS/PC composite and about a quarter of value of the PC control at 35 kW/m^2. Table I also shows that OPS and DOPO-POSS are better at reducing the THR of the PC matrix, but there is no obvious difference.

In Figures 1 and 2, the tendency to change temperature of the PC control is similar to the OPS/PC composite, but the DOPO-POSS/PC composite was different from them. And, from Figures 1 and 2, the top temperature curves indicate that the OPS/PC composite has a longer and more stable char forming process than the DOPO-POSS/PC composite. The thermal insulating effect of the char layer in the OPS/PC composite is far better than both the PC control and DOPO-POSS/PC composite.

At 35 kW/m^2, the temperature is so low that it could not make the specimen ignite quickly. There are two platforms in Figure 1 for the PC control and OPS/PC composite. The first platform is a sample-melting period. The second platform is a char layer forming period where the temperature remains stable until the char is broken, then the temperature begins to fall, because the top thermocouple was penetrated into the surface char layer which insulated the heat transfer. For the DOPO-POSS/PC composite, there is a short melting period, and then the temperature begins to drop down. One reason for this is that DOPO-POSS can accelerate the thermal decomposition of PC, and lead to early CO and CO_2 release from the matrix. Another reason is that the thermocouple may have penetrated into the matrix when the sample was melting, because the viscosity of the DOPO-POSS/PC composite is very low. At the same time, P-O radicals also existed in the gas products.[14] Many of the bubbles in the gas phase are broken when the temperature is rising, so the DOPO-POSS/PC composite has a shorter char formation period than the PC control and OPS/PC composite. The temperature change tendency of the bottom layer of the PC control is almost the same as that of the DOPO-POSS/PC composite, but the bottom temperature of the OPS/PC composite is much lower than both of them.

Figure 2 represents the data collected at 50 kW/m^2; it can be seen that the top temperature curve of the PC control is also similar to the OPS/PC composite, but there is only one platform left, and, along with Table I, this platform is the char formation platform of the PC control and OPS/PC composite. For the DOPO-POSS/PC composite, the top temperature curve is the same as the curve change at 35 kW/m^2. The char forming processes of both OPS/PC and DOPO-POSS/PC composites are longer than their char formation processes at 35 kW/m^2. At 50 kW/m^2, the bottom temperature of the PC control increases quickly until the char is broken, but the temperature still rises and does reach the top temperature. The bottom temperature of the OPS/PC composite is less than both the PC control and DOPO-POSS/PC composite.

Structure of Char Residue

The char layer photos of composites prepared at 35 kW/m^2 are shown in Figure 3. It can be seen that the char layer of the OPS/PC composite is wide and homogeneous, and there is some white SiO_2 powder on the surface. The char layer of DOPO-POSS/PC composite is sharp, loose, and concentrated in the center of the holder, which resulted in the heat deeply penetrating into the char layer.

Figures 4 and 5 show char residue photos of the OPS/PC and DOPO-POSS/PC composites prepared at 50 kW/m^2. The char shape of the OPS/PC composite is similar to that prepared at 35 kW/m^2, but the char layer shape of the DOPO-POSS/PC composite was lower and wider. At 50 kW/m^2, the char layer of the DOPO-POSS/PC composite is more dense and compact than the char prepared at 35 kW/m^2, but there are still many small holes at the exterior surface which prevented the heat

Table I. Cone Calorimeter Parameters of PC Control, DOPO-POSS/PC, and OPS/PC Composites

Heat flux (kW/m^2)	Sample	TTI (s)	TTF (s)	PHRR (kWm^2)	THR (MJ/m^2)
35	DOPO-POSS/PC	329	654	213	42
	OPS/PC	375	681	150	45
	PC control	336	551	572	76
50	DOPO-POSS/PC	95	480	235	62
	OPS/PC	80	549	208	56
	PC control	97	457	411	95

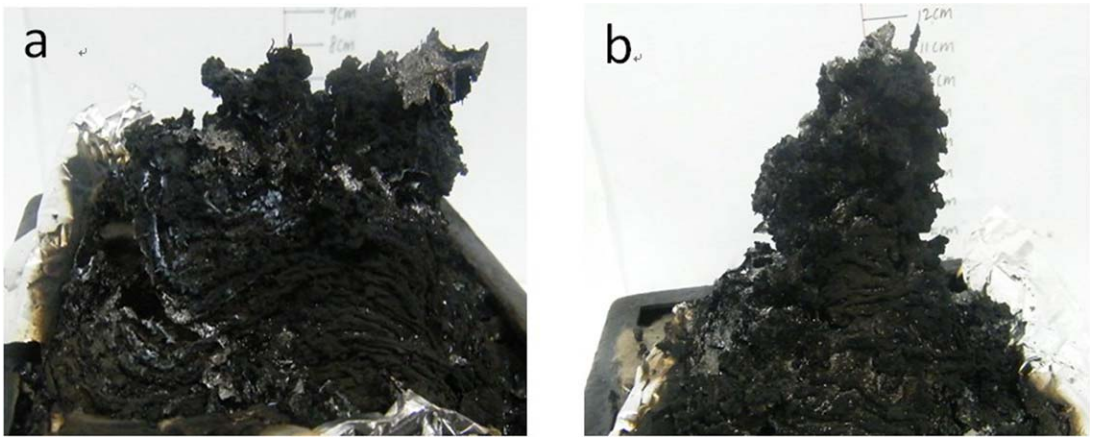

Figure 3. Photos of char layer at 35 kW/m^2: (a) OPS/PC composite (b) DOPO-POSS/PC composite. [Color figure can be viewed in the online issue, which is available at wileyonlinelibrary.com.]

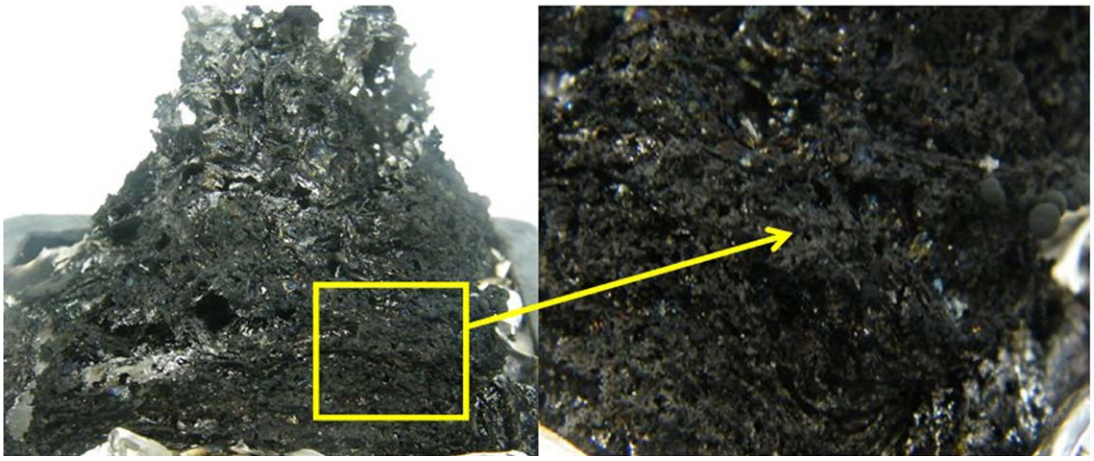

Figure 4. Photos of DOPO-POSS/PC composite char layer (50 kW/m^2). [Color figure can be viewed in the online issue, which is available at wileyonlinelibrary.com.]

from being released easily, resulting in a higher inside temperature than at 35 kW/m^2; this also resulted in heat entering the structure more easily. Figure 5 shows that there was more white SiO_2 powder covering the exterior of the OPS/PC composite compared with the photos of the char prepared at 35 kW/m^2. There is much more SiO_2 powder dispersed on the exterior and

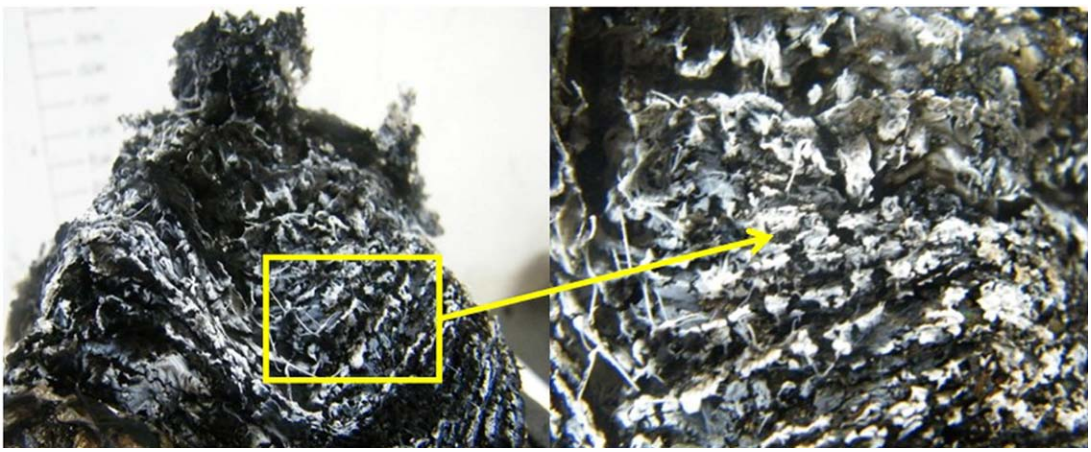

Figure 5. Photos of OPS/PC composite char layer (50 kW/m^2). [Color figure can be viewed in the online issue, which is available at wileyonlinelibrary.com.]

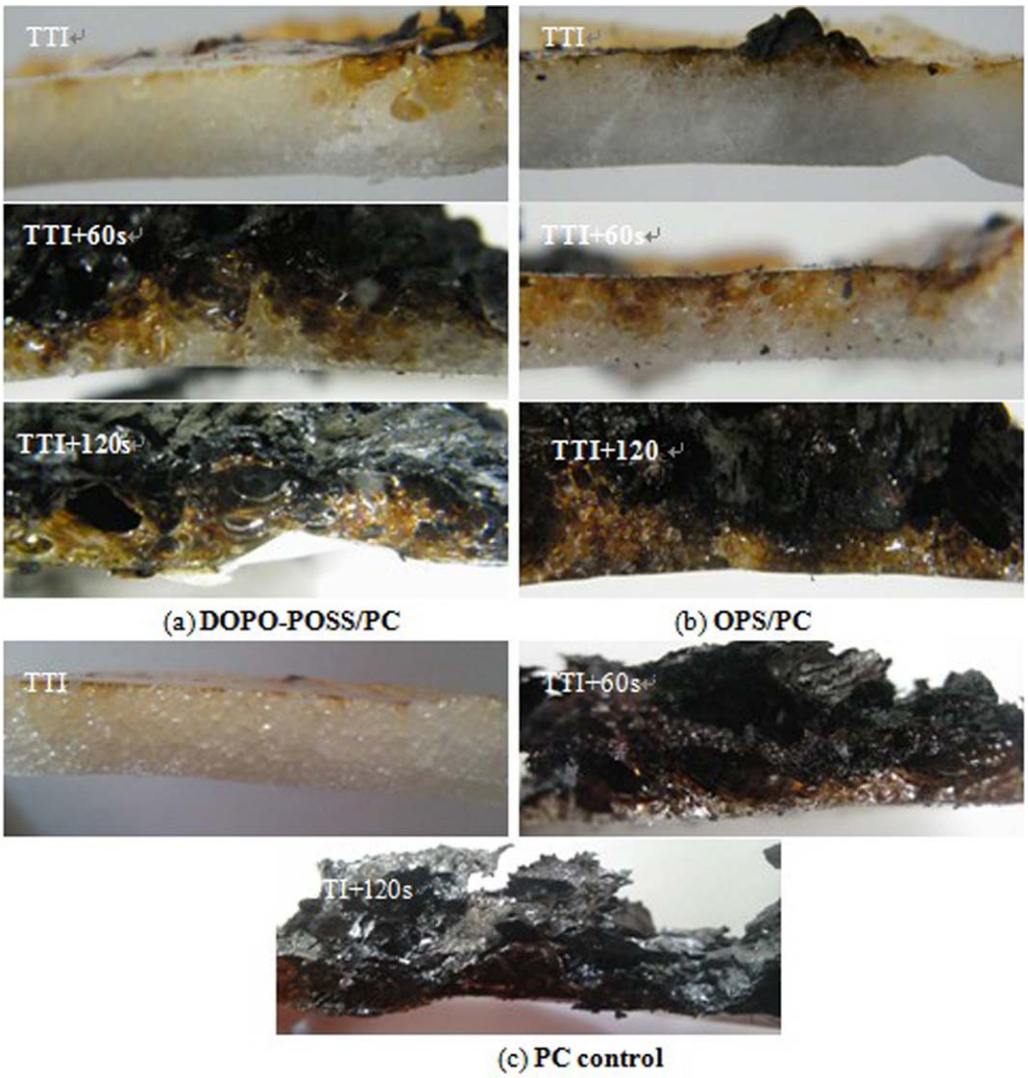

Figure 6. Photos of composites combustion at different time (50 kW/m^2). [Color figure can be viewed in the online issue, which is available at wileyonlinelibrary.com.]

it is evenly distributed over the surface, appearing wavy and more compact than the images in Figure 3.

Figure 6 shows the photos at TTI, TTI + 60 s, and TTI + 120 s during the composite combustions at 50 kW/m^2.

At TTI, Figure 6(a) had some big air holes near the surface and the sample became a faint yellow color and it appeared loose. Figure 6(b) only shows some small air holes near the surface, moreover the subsurface color did not change beneath the surface. Figure 6(c) shows the cross section photo of the PC control, and it shows that there were many bubbles inside the PC control compared with the OPS/PC and DOPO-POSS/PC composites. This indicates that heat can permeate the PC matrix quickly and promote sample loosening and degradation before TTI.

At TTI + 60 s, it can be seen that the DOPO-POSS/PC composite generated lots of bubbles beneath the surface, and the color of the combustion product became dark. However, the color of OPS/PC at TTI + 60 s is dark yellow near the surface, and the bubbles are bigger than at TTI. The white matrix at the bottom was also viewable. The PC control burned completely and only a thin matrix was left compared with the DOPO-POSS/PC and OPS/PC composites at TTI + 60 s.

At TTI + 120 s, the combustion product of the DOPO-POSS/PC composite has almost become a char residue. There are many bubbles in the interior char and no white matrix left. In Figure 6(b), the visible bubbles cannot be seen during the combustion period of the OPS/PC composite, and some melted matrix still existed at the bottom of the sample. In Figure 6(c), the PC control has been burned completely and it formed a loose char layer.

Figure 6 reflects the combustion image morphology of the three samples during the entire combustion process. It can be seen that the PC control is easier to degrade than the DOPO-POSS/PC and OPS/PC composites, and the DOPO-POSS/PC composite generated many bubbles during the combustion. The

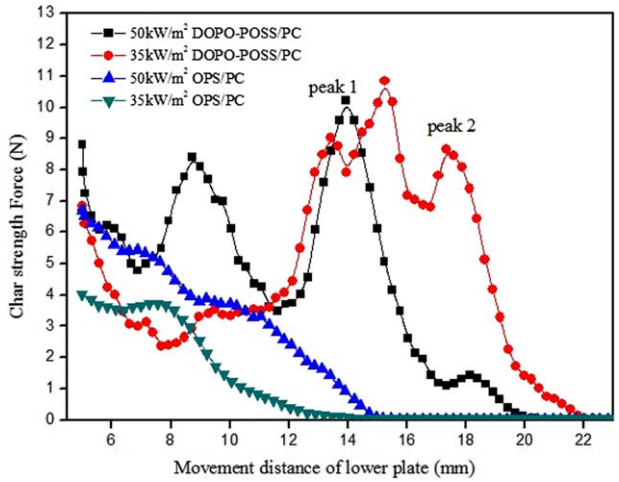

Figure 7. Strength of char at different heat fluxes. [Color figure can be viewed in the online issue, which is available at wileyonlinelibrary.com.]

combustion of the OPS/PC composite is slower and has a longer char formation stage. In comparison with the PC control and DOPO-POSS/PC composite, the OPS/PC composite at TTI + 60 s and TTI + 120 s indicate that the char layer can effectively prevent heat penetration into the interior matrix and make the bottom temperature rise slowly, and this result is consistent with Figure 2.

Strength of Char Residue

The strength of the char samples was obtained by cone test and the char strength curves are shown in Figure 7.

Figure 7 shows that the char layer strength of the DOPO-POSS/PC composite is stronger than that of the OPS/PC composite at both 35 and 50 kW/m^2. This is because a number of Si–O–phenyl and P–O–phenyl structures exist in the char residue of the DOPO-POSS/PC composite,[14–16] but there are only Si-O bonds left in the char of the OPS/PC composite. In Figure 7, peaks 1 and 2 in the DOPO-POSS/PC composite indicate that the DOPO-POSS/PC composite char layer was broken when it was pressed. The sharp peaks indicate that there are many holes in the interior char. When the holes are broken, the strength of char begins to decrease. The curve of the DOPO-POSS/PC composite indicates that the char layer is stronger at 50 kW/m^2 than at 35 kW/m^2, and the strength can reach 9 N at 35 kW/m^2 and 11 N at 50 kW/m^2. For the OPS/PC composite, the char at 50 kW/m^2 is stronger than at 35 kW/m^2 and the curves are similar to each other. The strength of the OPS/PC composite shows a gentle increase from 23 mm to 5 mm. However, the curves of the OPS/PC composite do not have sharp peaks, indicating that large holes do not exist in the OPS/PC char.

Based on the strength curves, the char layer of the OPS/PC composite is more compact and homogeneous than that of the DOPO-POSS/PC composite, but its char strength values at the different heat fluxes are lower than the corresponding DOPO-POSS/PC composite values.

SEM of Char Residue

The structure of the char that forms once the fire begins is very important to limit heat transfer. The exterior and fracture sections were taken from the of the char layers. Figures 8–11 show SEM char photos.

Figures 8 and 10 show the SEM photos of the interior char layer of the DOPO-POSS/PC and OPS/PC composites. It can be seen that there are many bubbles that attach to the internal char layers in the DOPO-POSS/PC composite. The bubbles are due to the gas released during combustion. In Figure 10(a), the size of the bubbles at 50 kW/m^2 is bigger than at 35 kW/m^2, indicating that all of the gas was released, resulting in increases in the total heat release, and this conclusion is confirmed by the cone test. But no bubbles or pores can be found in the interior char layer of the OPS/PC composite, and the char layer exhibits a laminated structure which means the char layer is more compact and orderly. Due to the existence of bubbles and pores, the heat could penetrate into the bottom layer easily. This is a reason why the bottom temperature of the DOPO-POSS/PC composite is higher than in the OPS/PC composite.

In Figure 9, there are many tiny and homogeneous pores distributed along the entire surface at 35 kW/m^2. However, the pores become disordered and large at 50 kW/m^2. The exterior char of the OPS/PC composite is compact and it condensed into a clump at both heat fluxes and the char looks like a compact net at 50 kW/m^2.

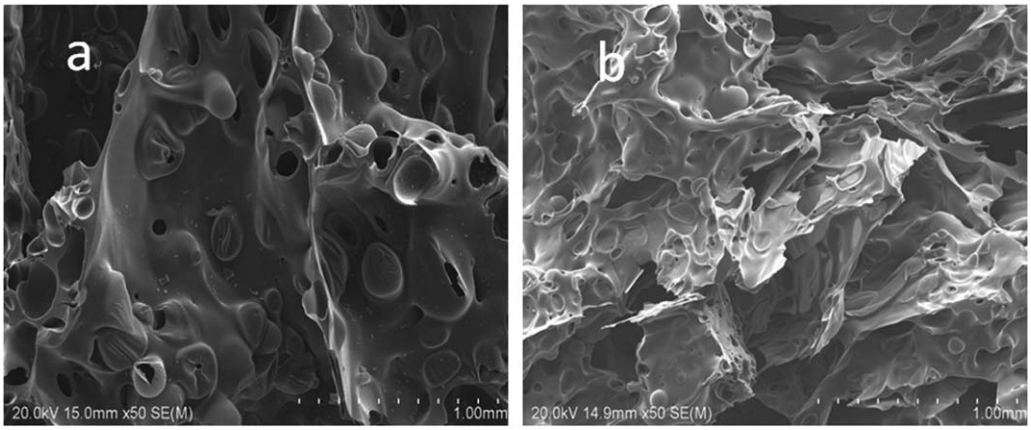

Figure 8. SEM photos of interior char layer at 35 kW/m^2: (a) DOPO-POSS/PC composite and (b) OPS/PC composite.

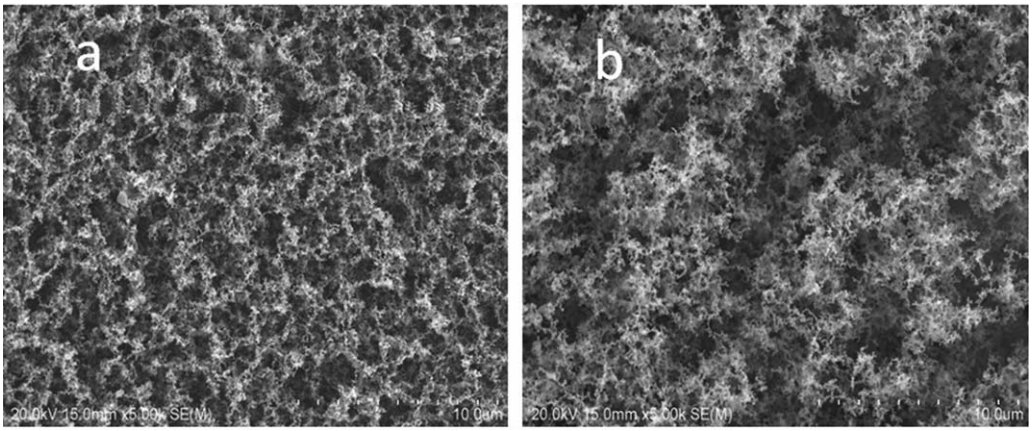

Figure 9. SEM photos of exterior char layer at 35 kW/m^2: (a) DOPO-POSS/PC composite and (b) OPS/PC composite.

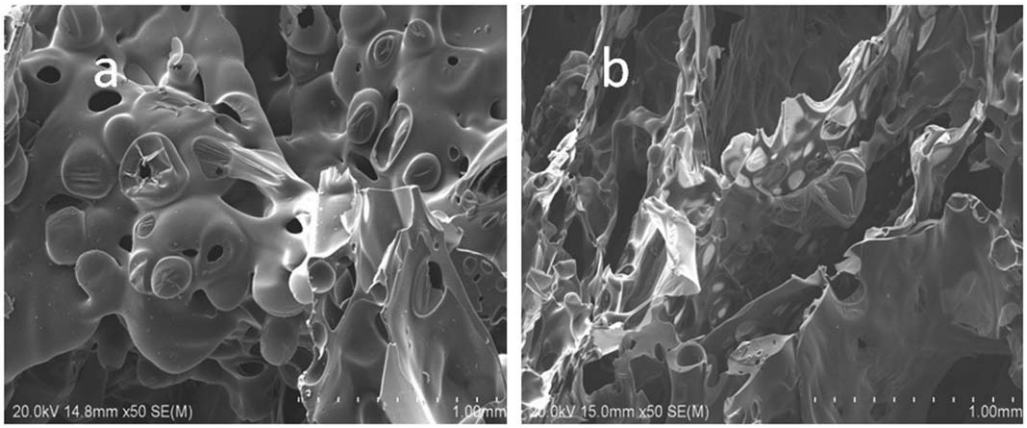

Figure 10. SEM photos of interior char layer at 50 kW/m^2: (a) DOPO-POSS/PC composite and (b) OPS/PC composite.

The presence of C, O, and Si elements in the char of the composites was determined from the cone calorimeter test. Table II shows the mass fraction of C, O, and Si elements in the exterior and interior surfaces of the char residue of the OPS/PC and DOPO-POSS/PC composites at different heat fluxes. At 35 kW/m^2, it can be seen that there is less Si content in the exterior and interior of the DOPO-POSS/PC composite, but the interior Si content is higher than that in the exterior. The interior Si content of the OPS/PC composite is also higher than its exterior, because the OPS/PC composite cannot be burned

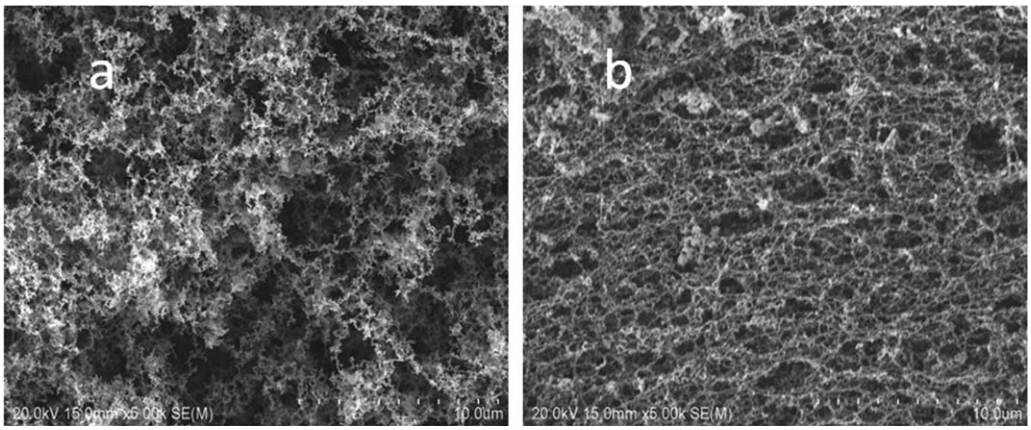

Figure 11. SEM photos of exterior char layer at 50 kW/m^2: (a) DOPO-POSS/PC composite and (b) OPS/PC composite.

Table II. Contents of C, O, Si Elements in the Char Residue from SEM-EDS

Heat flux (kW/m^2)	Composites		C (wt %)	O (wt %)	Si (wt %)
35	DOPO-POSS/PC	Exterior	76.52	22.34	1.14
		Interior	72.12	25.37	2.51
	OPS/PC	Exterior	72.93	20.71	6.36
		Interior	71.64	16.96	11.4
50	DOPO-POSS/PC	Exterior	79.32	20.3	0.38
		Interior	76.49	20.16	3.35
	OPS/PC	Exterior	19.53	48.26	32.21
		Interior	81.82	16.17	2.01

completely after being ignited. At 50 kW/m^2, the exterior Si content of the DOPO-POSS/PC composite is also lower than the interior Si content, but the exterior Si content of OPS/PC is much higher than the interior content. It is noted that the exterior char of the OPS/PC composite at 50 kW/m^2 is highly oxidized under the rich oxygen condition, and a number of Si–O bonds are in the exterior char. A number of Si elements are observed in the char residue of the OPS/PC composite which is helpful for the enhancement of the thermo-stability of the char.[17].

Rheological Analysis

Some studies showed a close relationship between viscoelastic characteristics and the flammability properties of thermoplastic-based polymer nanocomposites.[18–20] The storage modulus G' provides a method for understanding nanocomposite "stiffness," and its frequency dependence characterizes whether the material is in a liquid-like or solid-like state.[21] The relations between G' and G'' are shown in Figure 12 for the three samples. It can be observed that G' and G'' of the PC control and DOPO-POSS/PC composites increase with the rotational frequency and G'' is always higher than G' during the tests. For the OPS/PC composite, G' is little higher than G'' at low frequencies and it exhibits a solid-like state. This shows that the addition of OPS can improve the elasticity of PC. However, DOPO-POSS does not have such an effect. The DOPO-POSS/PC composite exhibits a typical liquid-like ($G' < G''$) characteristic corresponding to the formula $G' \propto \omega^2$ (where ω is the oscillatory frequency). For the OPS/PC composite, it is also observed that G' becomes nearly constant at low frequencies; this indicates a transition from a liquid to an ideal Hookean solid, which accompanies the formation of a mechanically stable network structure.[22–24]

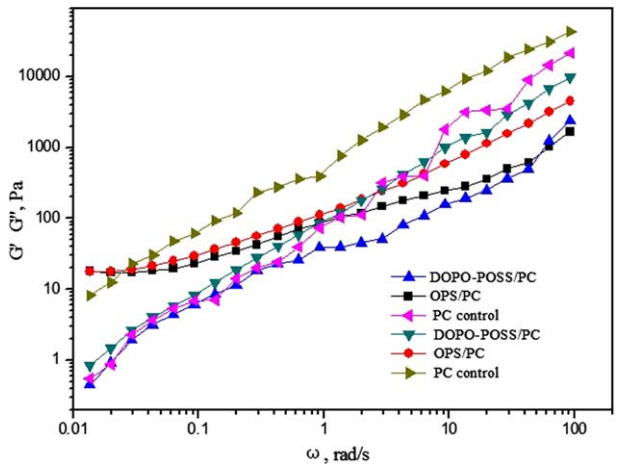

Figure 12. (a) Storage and (b) loss modulus versus angle frequency for OPS/PC composite, DOPO-POSS/PC composite and PC at 290°C. [Color figure can be viewed in the online issue, which is available at wileyonlinelibrary.com.]

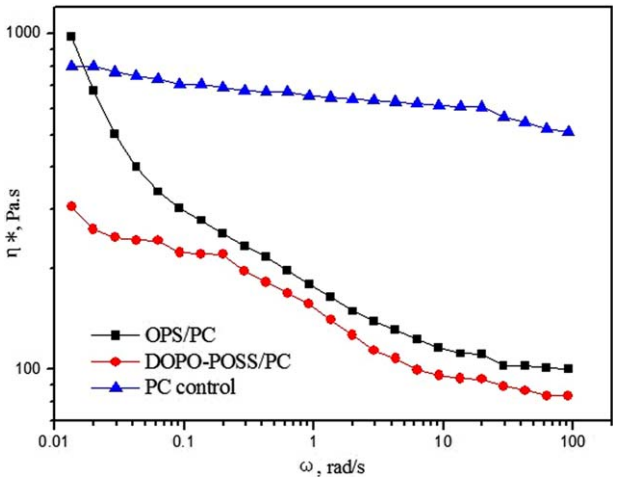

Figure 13. Complex viscosity versus angle frequency for OPS/PC composite, DOPO-POSS/PC composite, and PC control at 290°C. [Color figure can be viewed in the online issue, which is available at wileyonlinelibrary.com.]

The complex viscosity (η^*) values of the PC control, DOPO-POSS/PC and OPS/PC composites are shown in Figure 13. At low frequencies, the viscosity of the OPS/PC composite is higher than the PC control and DOPO-POSS/PC composite, which is coincident with the modulus curve. It can be seen that the PC control exhibits a quasi-Newtonian regime during the test, and shearing stress has little influence on its viscosity. However, the DOPO-POSS/PC and OPS/PC composites exhibit typical shear-thinning behavior during melted polymer flow, but the η^* of the OPS/PC composite was always higher than that of the DOPO-POSS/PC composite, which indicates that the OPS/PC composite behaves similarly to solid-like rheological behavior. This confirms that, under combustion conditions, the high melt viscosity could restrict the combustible gas release during the thermal degradation process and help the condensed phase to crosslink during char formation. Therefore, the OPS/PC composite can form a more stable char layer.

CONCLUSIONS

In cone calorimeter analysis, the OPS/PC composite has a longer char formation process than the DOPO-POSS/PC composite. The top temperature of the DOPO-POSS/PC composite decreased suddenly before the sample was ignited, then it continued to increase and then it experienced a short char formation. The bottom temperature of the OPS/PC composite

is much lower than the PC control and DOPO-POSS-PC composite.

In SEM analysis, some large holes and lots of bubbles remained in the interior char of DOPO-POSS/PC composite, and a loose char structure was observed. The color of the DOPO-POSS/PC composite became dark rapidly after ignition compared with the PC control and OPS/PC composite.

The most compact and orderly char layer is found in the OPS/PC composite. A number of white SiO_2 products covered the exterior char OPS/PC composite, but the DOPO-POSS/PC composite did not have such a phenomenon. The SiO_2 content in the surface of the OPS/PC char layer increased as the heat increased. The char strength of DOPO-POSS/PC is greater than that of the OPS/PC composite.

In rheological analysis, the DOPO-POSS/PC composite exhibited a liquid-like characteristic, and the OPS/PC composite exhibited a solid-like behavior. The η^* of the OPS/PC composite was higher than those of the PC control and DOPO-POSS/PC composite, which means the high melt viscosity could restrict combustible gas release during the thermal degradation process and help the condensed phase to crosslink during char formation under combustion conditions; this promotes PC to form a more stable char network structure.

REFERENCES

1. Levchik, S. V.; Weil, E. D. *Polym. Int.* **2005**, *54*, 981.
2. Chow, W. S.; Neoh, S. S. *J. Appl. Polym. Sci.* **2009**, *114*, 3967.
3. He, Q. L.; Song, L.; Hu, Y.; Zhou, S. *J. Mater. Sci.* **2009**, *44*, 1308.
4. Laine, R. M. *J. Mater. Chem.* **2005**, *15*, 3725.
5. Baney, R. H.; Itoh, M.; Sakakibara, A.; Suzuki, T. *Chem. Rev.* **1995**, *95*, 1409.
6. Li, G. Z.; Wang, L. C.; Ni, H. L.; Pittman, C. U. *Inorg. Organomet. Polym.* **2001**, *11*, 123.
7. Liu, L.; Hu, Y.; Song, L.; Nazare, S.; He, S. Q.; Hull, R. *J. Mater. Sci.* **2007**, *42*, 4325.
8. Fina, A.; Tabuani, D.; Camino, G. *Eur. Polym. J.* **2010**, *46*, 14.
9. Fina, A.; Abbenhuis, H. C. L.; Tabuani, D.; Camino, G. *Polym. Degrad. Stab.* **2006**, *91*, 2275.
10. Sanchez-Soto, M.; Illescas, S.; Milliman, H.; Schiraldi, D. A.; Arostegui, A. *Macromol. Mater. Eng.* **2010**, *295*, 846.
11. Li, L. M.; Li, X. M.; Yang, R. *J. Appl. Polym. Sci. J* **2011**. DOI:10.1002/app.35443.
12. Zhang, W. C.; Yang, R. J. *J. Appl. Polym. Sci.* **2011**, *122*, 3383.
13. Zhang, W. C.; Li, X. M.; Guo X. Y.; Yang, R. *J. Polym. Degrad. Stab.* **2010**, *95*, 2541.
14. Zhang, W. C.; Li, X. M.; Yang, R. J. *J. Appl. Polym. Sci.* **2012**, *124*, 1848.
15. Zhang, W. C.; Li, X. M.; Li, L. M.; Yang, R. *J. Polym. Degrad. Stab.* **2012**, *97*, 1041.
16. Zhang, W. C.; Li, X. M.; Fan, H. B.; Yang, R. *J. Polym. Degrad. Stab.* **2012**, *97*, 2241.
17. Chow, W. S.; Neoh, S. S. *J. Appl. Polym. Sci.* **2009**, *114*, 3967.
18. Takashi, K.; Minfang, M.; Karen, W.; Bani, C.; Raghavan, S. R.; Seongchan, P.; Miriam, R.; Yin, Y. *Polymer* **2008**, *49*, 4358.
19. Bartholmai, M.; Schartel, B. *Polym. Adv. Technol.* **2004**, *15*, 355.
20. Ma, H.; Tong, L.; Xu, Z.; Fang, Z. *Polym. Degrad. Stab.* **2007**, *92*, 1439.
21. Kharchenko, S. B.; Douglas, J. F.; Obrzut, J.; Grulke, E. A.; Milger, K. B. *Nat. Mater.* **2004**, *3*, 564.
22. Du, F.; Scogna, R. C.; Zhou, W.; Brand, S.; Fischer, J. E.; Winey, K. I. *Macromolecules* **2004**, *37*, 9048.
23. Bicerano, J.; Douglas, J. F.; Brune, D. A. *JMS Rev. Macromol. Chem. Phys.* **1999**, *C39*, 561.
24. Hobbie, E. K.; Fry, D. J. *J. Chem. Phys.* **2007**, *126*, 124907.